Chiral Self-Propulsion of Growing Bacterial Macrofibers on a Solid Surface

Neil H. Mendelson,[1] Joelle E. Sarlls,[2] Charles W. Wolgemuth,[2] and Raymond E. Goldstein[2,3]

[1]*Department of Molecular and Cellular Biology, University of Arizona, Tucson, Arizona 85721*
[2]*Department of Physics, University of Arizona, Tucson, Arizona 85721*
[3]*Program in Applied Mathematics, University of Arizona, Tucson, Arizona 85721*

(Received 26 August 1999)

Supercoiling motions that accompany the growth of bacterial macrofibers (multicellular filamentous structures formed in *B. subtilis* by cell division without separation) are responsible for rolling, pivoting, and walking of fibers on a surface. Fibers possess a fulcrum about which they pivot and step in a chiral manner; forces and torques associated with cell growth, when blocked by friction, result in self-propulsion. The elastic engine that drives macrofiber motions generates torques estimated as μdyn cm and femtowatts of power; optical trapping studies yield a first direct measurement of the Young's modulus of the bacterial cell wall, the engine's "working fluid," of ca. 0.05 GPa.

PACS numbers: 87.16.–b, 46.70.Hg, 47.15.Gf, 87.17.–d

This Letter focuses on the discovery that supercoiling motions of growing multicellular bacterial structures result in chiral self-propulsion when they are in contact with a solid surface. These structures, termed *macrofibers*, arise by repetitive supercoiling of an elongating chain of linked cells (a *filament*) or filament bundle that twists as it grows [1]. Individual rodlike cells, 4 μm $\times$ 0.7 μm, grow only in length, so the cell filaments, produced in a mutant of *B. subtilis* by failure of cell separation after each growth and division cycle, are of uniform diameter. They self-assemble into macrofibers millimeters in length and tenths of millimeters in diameter [2]; the mature structure consists of a single long filament folded repeatedly upon itself and twisted into a fiber shaft that is capped at both ends with loops. Macrofiber helix hand and degree of twist are governed by genetic and environmental factors such as temperature and the concentration of certain ions in the growth fluid [3].

The results reported here show that the twisting and writhing dynamics underlying supercoiling can constitute the workings of an *elastic engine* that powers chiral self-propulsion. Unlike other self-propulsion systems that operate at low Reynolds numbers and are based upon periodic movement of objects with fixed underlying shape or shape sequences [4], such as helical flagella turned by rotary motors or flexible flagella driven by local or distributed bending moments [5], macrofiber motions require increase in length. Several qualitative models have been advanced to explain the origin of twisting and supercoiling associated with growth [2,6–8]. The assembly of peptidoglycan, the strength-bearing cell wall polymer, is believed essential [6,9], but no definitive link between microscopic properties, such as the geometry of glycan orientation in the wall or its viscoelasticity, and the filament twisting with cell elongation has yet been established. A molecular model thus cannot yet be offered for the workings of this macrofiber elastic engine. By characterizing its output we hope to learn more about the ways in which it powers fiber self-assembly and other kinds of work, and also shed light on the polymer physics of bacterial cell walls and its link to cell growth.

Supercoiling of bacterial filaments may occur with *open* strands, thus in the absence of the topological constraint of fixed linking number that plays so crucial a role in the conformation [10] and dynamics of DNA and other twisted filaments [11]. Bacterial filaments are so stiff that the thermal fluctuations important in the statistical mechanics of DNA [12] also play no role. With fiber lengths typically on the order of 0.05 cm and velocities of 2×10^{-3} cm/s, the Reynolds number is at most $\mathcal{O}(10^{-2})$, so these phenomena occur without inertia—purely through a balance between elastic, body, and viscous forces.

The macrofibers used in these studies cannot swim or swarm, and no visible flagella structures can be found on their cell walls. They are, however, capable of slow movement over solid surfaces. Fibers make contact with the floor of a growth chamber because they are slightly denser than the growth medium in which they move. To study fiber motions on a surface a dual-view microscope system was constructed that permits simultaneous visualization of fiber contact with the surface and location within the chamber (Fig. 1). The growth chamber was illuminated both from below and the side with two light pipes from a single fiber optic light source (Dolan-Jenner, Inc.). Videos were made using two CCD cameras (Cohu); one fitted to an Olympus SZ-Tr zoom stereo microscope above the growth chamber, the other to a Bausch & Lomb monocular compound microscope tube aimed horizontally. The side-view images obtained from the latter always appear as mirror images due to reflection by the glass surface upon which the bacterial structures rest. Images were transferred to a Phase Eight screen splitter (Vicon Industries, Inc.) and the synchronized output sent to a GYYR time-lapse recorder (Odetics, Inc.). Motion dynamics were measured by comparison of individual frames directly using overlays on a video monitor screen, or following transfer to a PC using Image Pro Plus software (Media Cybernetics).

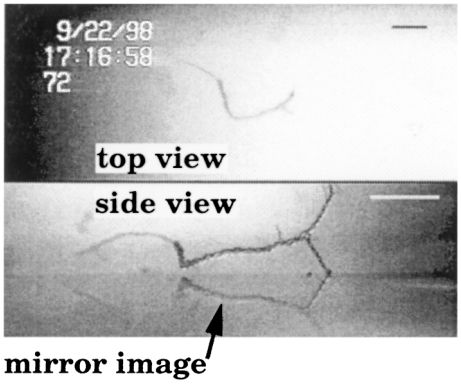

FIG. 1. Images of macrofibers from top and side within a glass growth chamber. Scale bar is 0.5 mm.

Motions of both right-handed (RH) and left-handed (LH) structures were examined [13] using *Bacillus subtilis* strains FJ7 and RHX [14]. Right-handed FJ7 fibers were produced by overnight growth in 10 ml of TB [15] containing $5 \times 10^{-2} M$ $MgSO_4$ at 20 °C. A single intact fiber was transferred into medium of the same composition in the glass growth chamber and the top was covered with two glass slides. For petri dish cultures, viewed only from above, a single fiber was disrupted by toothpick transfer into medium of the same composition. Both glass chamber and petri dish cultures were grown on a microscope stage at 24 °C. Left-handed RHX fibers were produced similarly using TB containing $5 \times 10^{-2} M$ $(NH_4)_2SO_4$.

Macrofibers underwent three kinds of motions as they grew on a solid surface: rolling, pivoting, and walking. Figure 2 shows that rolling is caused by twisting of a fiber about its shaft as it elongates. If the shaft and its terminal loop lie flat on the surface, twisting and friction result in propulsion. The terminal loop rises onto its edge then returns to the floor upside down at a slightly displaced position. The net result is rolling in a direction determined by the handedness of helix twisting. In Fig. 2, the lower half of each panel (the side view) shows the terminal loop of a right-hand fiber viewed end-on as it rolled to the left through 270° while the loop twisted in a counterclockwise direction. The corresponding top view images (upper half of each panel) reveal that during this sequence the fiber shaft pivoted clockwise. Other, low-magnification films show that the entire fiber shaft pivots in a helix-hand-specific direction (RH fibers clockwise, LH fibers counterclockwise). Rolling and pivoting are therefore inherent properties of macrofiber hand, not products of convection currents or other external forces.

Pivoting motions reveal that fibers possess a fulcrum midway along their length that effectively divides them into two mechanical halves [13]. During growth each half rotates in a direction opposite to the other. Figure 3a shows rates of clockwise and counterclockwise pivoting in RH and LH structures, respectively. Figure 3b shows

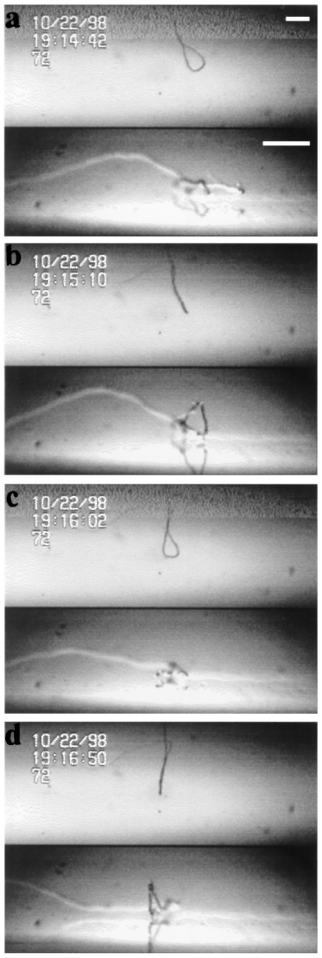

FIG. 2. Rolling sequence. Dual-view images showing motion of a macrofiber. Panels are at times (b) 28 s, (c) 80 s, and (d) 128 s after (a). Scale bar is 0.5 mm.

the corresponding rates of fiber length increase during pivoting. Repetitive periodic supercoiling, required for macrofiber morphogenesis, is responsible for the length reduction shown in Fig. 3b (the right-hand structure). After each supercoiling the newly formed structure must increase its length again before it undergoes another supercoiling and length reduction [6]. A symmetry argument can be advanced to explain the direction of fiber pivoting (Fig. 3c). There are two fundamental vectors in the problem, the surface normal **n** about which pivoting occurs at the fulcrum marked by a dashed line in Fig. 3c and the helicity vector **h** defining the twisting direction of the fiber. The pivoting vector **p** should be composed of these; the unique choice is $\mathbf{p} = \mathbf{n} \times \mathbf{h}$, which lies in the plane pointing in the direction that the frictional force of the surface acts to oppose the twisting motion. The vectors **p** so constructed for the two fiber ends are in opposite directions, leading to rotational motion. A composite of images taken from above (Fig. 3d) illustrates the overall pivoting motion. Both rolling and walking motions of half-fibers drive pivoting. The steps taken during walking

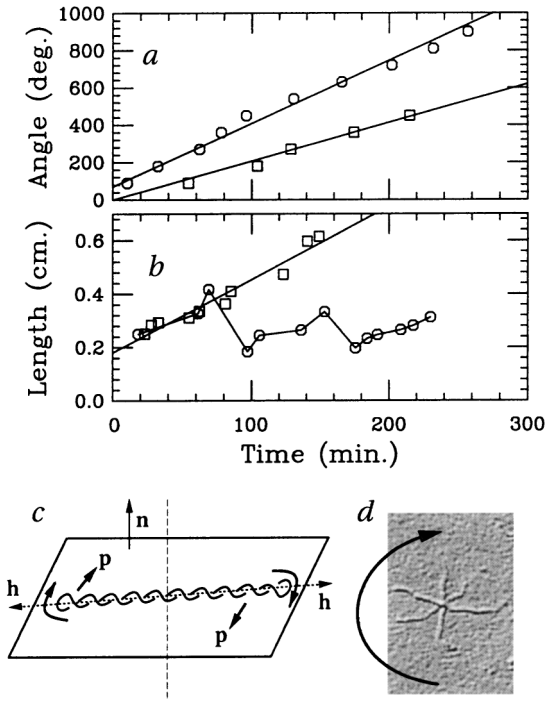

FIG. 3. Pivoting and fiber growth. (a) uniform rotational motion of left-handed (squares) and right-handed (circles) fibers, and (b) their length evolution, showing several folding events for the RH case. (c) Symmetry argument for angular direction of pivoting, with **n** the surface normal, **h** the helicity vectors (lying in the plane, along the plectoneme axis), and **p** the resultant pivoting forces, also in the plane. (d) Composite image from above showing pivoting around **n**.

(rectilinear motion) occur when part of a fiber rises off the surface and then returns to it elsewhere [13].

To determine the magnitude of viscous forces involved in fiber motion we model it as a straight, rigid rod rotating at angular speed ω about a pivot at one end. The force density acting on the fiber moving with local velocity v is $\zeta_\perp v = \zeta_\perp \omega s$ where s is the distance along the fiber from the pivot, $\zeta_\perp \simeq 4\pi\eta/\ln(L/a)$ is the drag coefficient for motion perpendicular to the fiber axis [16], η is the fluid viscosity, L is the fiber length, and a is its radius. The torque per unit length $\zeta_\perp \omega s^2$ yields a total torque $\tau_\perp = \zeta_\perp \omega L^3/3$. Data on two separate walking motions yield $\omega = 0.103$ rad $\cdot$ s^{-1} with $L = 0.73$ mm, and $\omega = 0.029$ rad $\cdot$ s^{-1} with $L = 1.65$ mm. The corresponding torques are 1.7×10^{-6} erg and 5.4×10^{-6} erg, respectively. Both are significantly larger than gravitational torques acting on the structures studied, estimated by the same reasoning to be $\tau_g \simeq \pi a^2 \delta\rho g L^2/2 \simeq 6 \times 10^{-7}$ erg, where $\delta\rho$ is the density difference between the fiber of radius $a \simeq 0.002$ cm and the surrounding fluid [17].

Continuing in this manner, we estimate the power generation by these motions to be $P = \tau_\perp \omega$. With the values for L, ω, etc., used above we find $P \sim 2 \times 10^{-14}$ W. Scaling by the filament volume the power density is approximately 20 nW/cm^3. For comparison, the power generated by 1 μm spherical bacterium swimming at 10 μm/s is about 500 nW/cm^3.

Macrofiber self-assembly and the unique motions described here are made possible by the elastic nature of *B. subtilis* cells, that is the material properties of peptidoglycan. This is the "working fluid" of the elastic engine, undergoing repeated elongation and buckling (supercoiling). Even its most basic material properties have not been determined in any direct manner, although studies of large man-made aggregate structures called bacterial thread give estimates of the Young's modulus [18], which ultimately sets the scale for the propulsive forces. We have determined the bending modulus of single cell filaments from their relaxation [19] after deformation by an optical trap, constructed [20] from a 400 mW $NdYVO_4$ diode laser (1.064 μm) (SantaFe Lasers), telescopic beam expansion, motorized steering lenses under computer control (LabView, National Instruments), and a Nikon Diaphot 300 inverted microscope with an oil-immersion plan-apo 100$\times$ (NA 1.4) objective. To increase trapping strength over that achievable with bare filaments, 2 μm diameter latex beads (Ernest F. Fullam) were attached to the filament tip after incubation for 10 min in a 0.01M solution of polylysine (Sigma) and several cycles of rinsing. Attachment was achieved by moving a trapped bead into contact with the filament, which was then bent by steering the trap; when the elastic restoring force of the filament exceeded the trapping force, the bead-filament assembly escaped the trap and relaxed. Movies of the bead motion were analyzed using locally written centroid-tracking software based on a standard algorithm [21].

The relaxation of the filament tip position $h(t)$ is of the form $h_0 \exp(-\sigma t)$, where $\sigma = Ak^4/\zeta_\perp$, where A is the single-filament bending modulus and k is the first allowed wave number associated with clamped-free boundary conditions for an elastica [19]. Figure 4 shows a typical relaxation curve and its fit to this functional form. From tens of runs on filaments of lengths from 10–50 μm, we find $A \simeq (1.6 \pm 0.6) \times 10^{-12}$ erg cm. Assigning a persistence length by the relation $A = k_B T L_p$ we find $L_p \sim 40$ cm, almost 2 orders of magnitude larger than that of microtubules [22]. Using A to estimate the Young's modulus under the simplifying assumption that the stiffness is determined by the thin cell wall (with $A \simeq \pi a^3 t E$, with $t \simeq 25$ nm) we obtain $E \sim 0.05$ GPa, quite similar to that of rubber and remarkably close to that found earlier [18].

This single-filament bending modulus can be compared to that inferred from the torque estimates above on macrofibers. If we assume that the torque comes from twist built up in the fiber, then $\tau_{\text{twist}} \sim C_m \Omega$ where C_m is the twist elastic modulus of the macrofiber and Ω the twist density at the fulcrum. To execute the given motion, the twist must be greater than that needed to cause buckling.

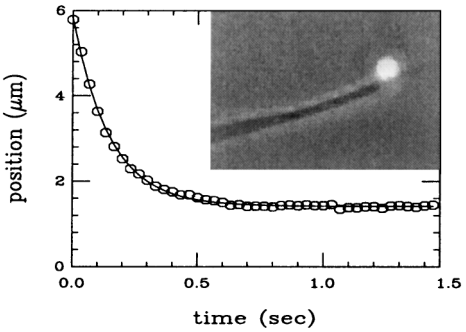

FIG. 4. Exponential relaxation of a bead attached to a fiber tip, following displacement by an optical trap. Inset shows a 2 μm bead attached to a filament.

Elasticity theory [23] yields the result that buckling occurs when $(C_m/A_m)\Omega L \approx 10$. Setting the twist torque equal to the torque necessary to oppose viscous drag and gravity yields $C_m \sim \tau L/10 \sim 10^{-7}$ erg cm, fully 5 orders of magnitude larger than the single filament bending modulus. Assuming, as with most materials, that the bend and twist moduli are comparable, and further invoking the expected scaling of moduli with (radius)^4 shows rough consistency between the filament and fiber data. Clearly, quantitative force measurements on macrofibers are needed, perhaps achievable using mechanical micromanipulation techniques such as deflection of needles of known compliance.

The macrofiber elastic engine transduces forces derived from cell growth into motions that accomplish three tasks: assembly of the multicellular fiber form, translational movement over a surface, and the pulling together of objects attached to a fiber's ends. The physics upon which the macrofiber engine operates should be applicable to other biological systems at scales ranging from molecular to multicellular dependent upon the elastic properties of the twisting filament and the environment within which it operates. Further measurements of forces and dynamics are clearly called for in the effort to formulate a more complete picture of this elastic engine.

We thank S. D. Whitworth for technical support, and D. K. Warren, K. M. Williams, and N. E. Hartvigsen for video assistance. This work was supported by the NCRR, NIH (NHM), NSF Grant No. DMR9812526 (J. E. S. and R. E. G.), and the University of Arizona Undergraduate Biology Research Program (J. E. S.).

[1] N. H. Mendelson, Proc. Natl. Acad. Sci. U.S.A. **73**, 1740 (1976); **75**, 2478 (1978).

[2] N. H. Mendelson and J. J. Thwaites, Mater. Res. Soc. Symp. Proc. **174**, 171 (1990); N. H. Mendelson, Mater. Res. Soc. Symp. Proc. **255**, 43 (1992).

[3] N. H. Mendelson and D. Favre, J. Bacteriol. **169**, 519 (1987).

[4] S. Childress, *Swimming and Flying in Nature* (Cambridge University Press, Cambridge, 1981).

[5] G. I. Taylor, Proc. R. Soc. London A **211**, 225 (1952); E. M. Purcell, Proc. Natl. Acad. Sci. **94**, 11 307 (1997); C. H. Wiggins and R. E. Goldstein, Phys. Rev. Lett. **80**, 3879 (1998); S. Camalet, F. Jülicher, and J. Prost, Phys. Rev. Lett. **82**, 1590 (1999).

[6] N. H. Mendelson, J. Bacteriol. **151**, 438 (1982); D. Favre, N. H. Mendelson, and J. J. Thwaites, J. Gen. Microbiol. **132**, 2377 (1986).

[7] M. J. Tilby, Nature (London) **266**, 450 (1977).

[8] I. Klapper, J. Comput. Phys. **125**, 325 (1996); M. Tabor and I. Klapper, in *Mathematical Approaches to Biomolecular Structure and Dynamics*, IMA Vol. 82, edited by J. P. Mesirov, K. Schulten, and D. W. Sumners (Springer-Verlag, New York, 1995).

[9] A. Zaritsky and N. H. Mendelson, J. Bacteriol. **158**, 1182 (1984); A. L. Koch, J. Theor. Biol. **141**, 391 (1989); *Bacterial Growth and Form* (Chapman & Hall, New York, 1995).

[10] F. B. Fuller, Proc. Natl. Acad. Sci. U.S.A. **75**, 3557 (1978); N. R. Cozzarelli, T. C. Boles, and J. White, in *DNA Topology and its Biological Effects*, edited by N. R. Cozzarelli and J. C. Wang (Cold Spring Harbor Laboratory, Cold Spring Harbor, New York, 1990); C. R. Calladine and H. R. Drew, *Understanding DNA. The Molecule & How It Works* (Academic Press, New York, 1992).

[11] I. Klapper and M. Tabor, J. Phys. A **27**, 4919 (1994); I. Klapper, J. Comput. Phys. **125**, 325 (1996); A. Goriely and M. Tabor, Phys. Rev. Lett. **77**, 3537 (1996).

[12] J. F. Marko and E. D. Siggia, Science **265**, 506 (1994); Phys. Rev. E **52**, 2912 (1995).

[13] Movies of the processes described here can be found at research.biology.arizona.edu/mendelson/mands.

[14] N. H. Mendelson, J. Bacteriol. **170**, 2336 (1988).

[15] TB consisted of 10 g of Bacto Tryptose (Difco), 3 g of Bacto Beef Extract (Difco), and 5 g of NaCl, each per liter of deionized water. See [3].

[16] J. Lighthill, *Mathematical Biofluiddynamics* (SIAM, Philadelphia, 1975).

[17] Fiber density at 24 °C in TB is 1.015 g/cm^3 from the sedimentation velocity $v \simeq (2/9)R^2\Delta\rho g/\eta$ of fiber-ball structures of radius R [N. H. Mendelson, B. Salhi, and C. Li, in *Bacteria as Multicellular Organisms*, edited by J. A. Shapiro and M. Dworkin (Oxford University Press, New York, 1997), p. 339], with η the viscosity, and $\Delta\rho$ the density difference, approximating the dense fiber-ball as a solid sphere.

[18] J. J. Thwaites and N. H. Mendelson, Adv. Microb. Physiol. **32**, 173 (1991).

[19] C. H. Wiggins, D. Riveline, R. E. Goldstein, and A. Ott, Biophys. J. **74**, 1043 (1998).

[20] K. Svoboda and S. M. Block, Annu. Rev. Biophys. Biomol. Struct. **23**, 247 (1994).

[21] J. Gelles, B. J. Schnapp, and M. P. Sheetz, Nature (London) **331**, 450 (1988).

[22] M. Elbaum, D. K. Fygenson, and A. Libchaber, Phys. Rev. Lett. **76**, 4078 (1996).

[23] See, e.g., L. D. Landau and E. M. Lifshitz, *Theory of Elasticity* (Pergamon Press, Oxford, 1986), 3rd ed.